Journal of Power Sources 241 (2013) 359–366

Contents lists available at SciVerse ScienceDirect

Journal of Power Sources

journal homepage: www.elsevier.com/locate/jpowsour

Synthesis and property of novel MnO_2@polypyrrole coaxial nanotubes as electrode material for supercapacitors

Wei Yao [a,b], Hui Zhou [a], Yun Lu [a,*]

[a] Department of Polymer Science and Engineering, State Key Laboratory of Coordination Chemistry, School of Chemistry and Chemical Engineering, Nanjing University, Nanjing 210093, PR China
[b] School of Materials Engineering, Yancheng Institute of Technology, Yancheng 224051, PR China

HIGHLIGHTS

- MnO_2@PPy coaxial nanotubes are prepared without surfactant and additional oxidant.
- The thickness of PPy outer layer deposited on MnO_2 nanotubes can be adjusted.
- A high specific capacitance of 380 F g^{-1} is obtained.
- Excellent rate capability and good capacitance retention are achieved.

ARTICLE INFO

Article history:
Received 7 March 2013
Received in revised form
26 April 2013
Accepted 26 April 2013
Available online 9 May 2013

Keyword:
Manganese oxide
Polypyrrole
Coaxial nanotubes
Supercapacitors
Synergic effect

ABSTRACT

Novel MnO_2@polypyrrole (PPy) coaxial nanotubes have been prepared via a simple and green approach without any surfactant and additional oxidant. Under the acidic condition, MnO_2 nanotubes act as both template and oxidant to initiate the polymerization of pyrrole monomers on its fresh-activated surface. Fourier transform infrared spectra (FT-IR), X-ray diffraction patterns (XRD), thermo-gravimetric analysis data (TG) and X-ray photoelectron spectra (XPS) suggest the formation of composite structure of MnO_2@PPy. Also, FESEM and TEM images intuitively confirm that the PPy shell is coated uniformly on the surface of MnO_2 nanotubes. Adjusting the concentrations of sulfuric acid or adding oxidant can modulate the morphology of the products accordingly. Due to the synergic effect between MnO_2 core and PPy shell, the MnO_2@PPy coaxial nanotubes possess better rate capability, larger specific capacitance of 380 F g^{-1}, doubling the specific capacitance of MnO_2 nanotubes, and good capacitance retention of 90% for its initial capacitance after 1000 cycles.

1. Introduction

Heterostructured nanomaterials such as coaxial nanowires/nanotubes, core/shell microspheres have attracted greater attention in the nanoscience research field due to their added synergic properties or functionalities derived from combining different materials [1–7]. For instance, various composite systems with core/shell structure, such as metal/metal [4], carbon/metal oxide [1], metal oxide/metal oxide [5], etc., have been prepared and tried to apply in different fields. Coaxial one-dimensional (1D) nanostructured materials may offer more novel properties and functions due to their anisotropy in structure and have also been both desirable and challenging for us [8].

As one of excellent alternate supercapacitor electrode materials, RuO_2 shows a limited commercialization because of its high cost and toxic nature [9]. By contrast, MnO_2 has attracted intensive studies on account of its high theoretical capacitance (1370 F g^{-1}), low cost, resource abundance and environmental friendliness [10–18]. Yet, actual electrochemical capacitance of MnO_2, unfortunately, is only in the range of 100–250 F g^{-1} [10–18], which is ascribed to the fact that owing to its poor electrical conductivity, only the surface layer of tens nanometers in thickness takes part in the charge storage process [19–21].

In order to improve the capacitance performance, many researches have paid close attention to synthesis of various nanostructures of MnO_2, such as hollow spheres [18,22], hollow urchins [22], nanowires/nanorods [10,13–15] and nanotubes [11]. Among these nanostructures, nanotube materials can provide not only high surface area and surface to volume ratio to contact with an electrolyte, thus affording short ion diffusion path and fast kinetics, but

* Corresponding author.
E-mail address: yunlu@nju.edu.cn (Y. Lu).

0378-7753/$ – see front matter © 2013 Elsevier B.V. All rights reserved.
http://dx.doi.org/10.1016/j.jpowsour.2013.04.142

also better accommodation of large volume change, increasing the cycle life [11,15]. Another strategy to consider is adding conducting agent, such as carbonaceous materials [23–26] and conducting polymers [2,6,7,19–21,27–35], to increase the conductivity of composite nanostructures. However, in the case of carbonaceous materials, the specific capacitance of MnO_2/carbon hybrid materials is relatively low, since the contribution of most carbonaceous materials to the capacitance is weak [33]. For conducting polymers such as polypyrrole (PPy), polythiophene (PTh) and polyaniline (PAn), their good conductive ability at the doping state, is beneficial to the increase of the electrons and ions exchange rate [6]. Moreover, the specific capacitance of conducting polymers is higher than carbonaceous materials [36,37], but ineffective at providing good rate capability and cycling performance [7]. So, with respect to the developing of supercapacitors, it is very significant to design an integrated smart architecture, in which the merits of each component can be optimized, to act as the high quality electrode material.

Up to now, several works concerning both MnO_2 and conducting polymers as well as their composite preparation for supercapacitor application has been published. For instance, by using pre-prepared MnO_2 nanowires as the reactive templates, the conducting polymer PPy nanotubes have been fabricated [38]. Also, one-dimensional nanostructured MnO_2/PPy composites have been prepared by in situ chemical oxidation polymerization of pyrrole in the host of inorganic matrix of MnO_2 using complex of methyl orange (MO)/$FeCl_3$ as a reactive self-degraded soft-template [31]. The ultrafine β-MnO_2/PPy nanorod powders have been synthesized via an in-situ co-precipitation approach by using pyrrole monomers as a reduction agent to reduce Mn^{7+} ions in $KMnO_4$ solution to form β-MnO_2 crystal and at the same time oxidating pyrrole monomers themselves to generate conductive PPy [19]. Moreover, ternary composite of carbon nanotube/PPy/MnO_2 [39,40] and MnO_2/PPy@carbon nanofiber triaxial nano-cables [41] have also been developed and exhibit the superior cycle life and rate capability. Even so, the research aimed at obtaining advanced electrode materials with excellent electrochemical property using simple and green preparation method as well as low fabrication cost is still necessary and important.

In this work, we present a novel nanostructure of MnO_2@PPy coaxial nanotubes prepared via a simple and green approach in the absence of any surfactant and additional oxidant. Under the acidic condition, MnO_2 nanotubes act as both template and oxidant to initiate the polymerization of pyrrole monomers on its fresh-activated surface. Moreover, the influences of acid concentration and additional oxidant, such as ferric trichloride ($FeCl_3$), on the morphologies of the MnO_2@PPy coaxial nanotubes have been also investigated. To the best of our knowledge, there have been few studies on MnO_2@PPy coaxial nanotubes for supercapacitors. In this work, the novel design of MnO_2@PPy coaxial nanotube structures, using as electrode material, has following advantages. Firstly, PPy could be well-grown on MnO_2 nanotubes, effectively enhancing the conductivity of composites, speeding electrons/ions diffusion. Secondly, MnO_2 nanotubes serve as backbone for PPy and also restrain the structural change of PPy in cycle process, thus enhancing cycling performance. Thirdly, both the core and shell materials are good electrode materials for supercapacitors, and their novel properties containing the characteristics of each of the components with a synergistic effect could promote the quality of the supercapacitors. And finally, there are no organic solvent and various additives in the reaction system, and the preparation procedures, for forming MnO_2 nanotubes and MnO_2@PPy coaxial nanotubes from the cheap $KMnO_4$ and pyrrole monomers, are straightforward and convenient just via hydrothermal synthesis and in-situ polymerization respectively, which provides a simple, economic and green approach to fabricate an important kind of metal oxide/conducting polymer nanocomposites that are potentially useful in high-tech fields.

2. Experimental

2.1. Materials

Pyrrole of analytical grade was purchased from Aldrich Chemical Co. and distilled under vacuum prior to use. All other reagents were received as analytical grade and were used without further purification.

2.2. Preparation of MnO_2 nanotubes

MnO_2 nanotubes were prepared referring to the method previously reported [11,42] with minor modification. In a typical process, 0.307 g $KMnO_4$ and 0.65 mL concentrated HCl were added into 35 mL deionized water to form the precursor solution. After rapidly stirring for 30 min, the solution was transferred to a Teflon-lined, stainless-steel autoclave with a capacity of 50 mL. The autoclave was sealed and kept in a blast electric oven at 140 °C for 12 h. After cooling down to room temperature naturally, the brown precipitates were filtered, and then washed by deionized water to remove possible impurities or excess ions. Finally, the as-prepared samples were dried at 100 °C in an oven for 12 h.

2.3. Preparation of MnO_2@PPy coaxial nanotubes

150 mg of the as-prepared MnO_2 nanotubes were dispersed in 60 mL 0.01 M H_2SO_4 aqueous solution under ultrasonic condition and then cooled in an ice bath with a slow stir. 100 μL pyrrole monomers were dissolved in 40 mL 0.01 M H_2SO_4 aqueous solution. These two newly prepared solutions were rapidly mixed and then stirred in an ice bath for 3 h. The generated black product was filtered, then washed with deionized water and ethanol several times, and finally dried at 60 °C for 12 h.

2.4. Materials characterization and electrochemical test

The morphologies of the samples were observed by field emission scanning electron microscopy (FESEM, Hitachi, S4800, Japan) and transmission electron microscopy (TEM, JEOL, JEM-200CX, Japan). In each TEM measurements, a drop of diluted sample was placed on a copper grid and evaporated prior to observation. The phase structures were identified by X-ray diffraction analysis (XRD, Shimadzu, XRD-6000, Japan) with Cu Kα radiation ($\lambda = 1.5418$ Å) at room temperature in the 2θ range of 10°–70°. Fourier-transform infrared spectra were recorded on a Bruker VECTOR22 spectrometer with 4 cm^{-1} resolution using pressed KBr pellets of samples in solid state. X-ray photoelectron spectra (XPS, ESCALB MK-II, VG Co., England) were performed under a base pressure of 1×10^{-9} Torr using monochromatic Mg Kα X-rays at $h\nu = 1253.6$ eV. Thermogravimetric analyses (TG) were run on a Pyris1 TGA instrument from room temperature to 800 °C at a heating rate of 10 °C min^{-1} under air. The electrical conductivity measurements were made on compaction of powder in pellet form by using the standard four-probe method at room temperature. The zeta-potential measurement of MnO_2 nanotubes was carried out by means of Malvern Zetasizer 3000HSA equipped with a 633 nm laser. The electrochemical measurements were carried out using three-electrode system in a 1 M Na_2SO_4 solution. The working electrodes were fabricated by pressing the homogeneous mixture that comprised the as-prepared samples, acetylene black and polytetrafluoroethylene (PTFE) blinder in a mass ratio of 80:10:10 on

foam nickel current collectors (1 × 1 cm) at 10 MPa and dried in vacuum at 120 °C for 12 h. Platinum foil and saturated calomel electrode (SCE) were used as the counter and reference electrodes respectively. All electrochemical measurements were performed on a CHI660B electrochemical workstation (Shanghai CH Instrument Company, China). The average specific capacitance values were calculated from the area of the CV plot according to Eq. (1) [15]:

$$C = \frac{i}{m \times \Delta V} \quad (1)$$

where m was the mass of active materials, ΔV was the potential sweep rate, i was the charge obtained through integrating the area of the cyclic voltammetry (CV) curve.

3. Results and discussion

In general, MnO_2 nano-materials prepared by hydrothermal method possess various morphologies and crystallographic phases [10,11,13–15]. Structurally, α-MnO_2 is constructed from double chains of octahedral [MnO_6] forming the 2 × 2 tunnels with a cavity of about 0.46 nm, which is fit for exchange of alkali cations in electrolyte and make the material suitable to act as electrode material in supercapacitors [11]. In contrast with bulk materials, 1-D nanotube structure can increase the surface area due to surface and boundary effect, shorten ion diffusion path and speed up ion and electron transfer. However, poor electrical conductivity of MnO_2 remains a major problem and results in lower specific capacitance. To improve it, many approaches are focused on forming MnO_2-conducting polymers composite nanostructures to increase the electrical conductivity of electrode material [21,29]. Fortunately, α-MnO_2 is known to work as a medium oxidizing agent in acidic environment (the standard electrode potential of MnO_2 is 1.23 V), which could initiate the polymerization of pyrrole monomers. Therefore, in our case, MnO_2@PPy coaxial nanotubes can be prepared in acidic environment, using α-MnO_2 nanotubes as both backbone and oxidant.

Fig. 1 shows the FESEM and TEM images of α-MnO_2 nanotubes and MnO_2@PPy coaxial nanotubes. It can be seen that, the as-prepared MnO_2 shows 1-D nanostructured crystals with clearly tetragonal open end (see the marked black square area in Fig. 1a), no other morphologies are observed in the sample. TEM image in Fig. 1c further confirms the formation of MnO_2 nanotubes with average outer diameter of 75 nm, average inner diameter of 25 nm and average length of several microns. Fig. 1b shows the FESEM image of the MnO_2@PPy coaxial nanotubes, in which the sample displays rough surface with length of about 1 μm and diameter of about 80 nm. Since the MnO_2 works as oxidant and template in the chemical reaction, the diameter of the MnO_2@PPy coaxial nanotubes has little change compared with MnO_2 nanotubes. TEM image in Fig. 1d clearly reveals the core/shell morphology of the MnO_2@PPy nanostructure with the outer layer of PPy with thickness about 15–20 nm and the inner layer of MnO_2 nanotubes with the wall thinned, confirming the successful preparation of MnO_2@PPy coaxial nanotubes.

In order to further prove the core/shell structure of MnO_2@PPy nanotubes, the XPS analysis is used to characterize the chemical component of MnO_2 and MnO_2@PPy coaxial nanotubes. In the N 1s region (Fig. 2a), the intense peaks at 399.4 eV, 397.6 eV and 402.0 eV correspond to the pyrrole nitrogen (−NH−), the imine-like (=N−) structure and positively charged nitrogen [43] respectively, indicating the existence of PPy. Moreover, the characteristic Mn 2p peaks disappear in Fig. 2b for the MnO_2@PPy coaxial nanotubes, suggesting that the PPy shell has been coated uniformly on MnO_2 nanotubes.

The phase purity and crystal structure of the MnO_2@PPy coaxial nanotubes have been identified by X-ray power diffraction techniques. As showed in Fig. 3a, all the diffraction peaks can be indexed with the standard XRD pattern of α-MnO_2 (JCPDS No. 44-0141, tetragonal symmetry with $I4/m$ space group and lattice constants of a = 9.7847 Å, b = 9.7847 Å and c = 2.6830 Å). No characteristic impurity peaks are observed, indicating the high purity of α-MnO_2 nanotubes. Seen from the XRD pattern of the MnO_2@PPy nanotubes

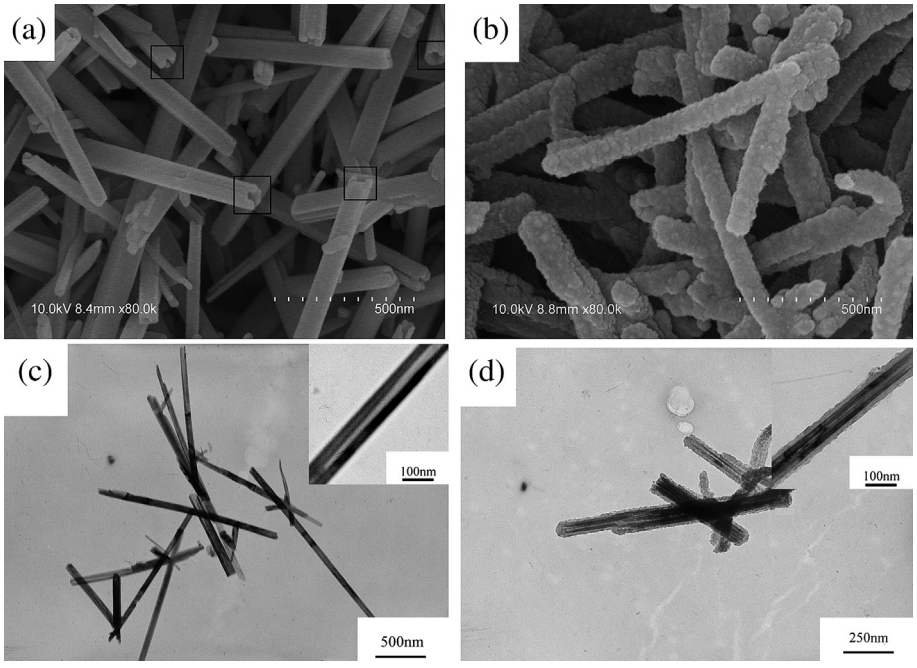

Fig. 1. FESEM images of (a) MnO_2 and (b) MnO_2@PPy nanotubes; TEM images of (c) MnO_2 and (d) MnO_2@PPy nanotubes.

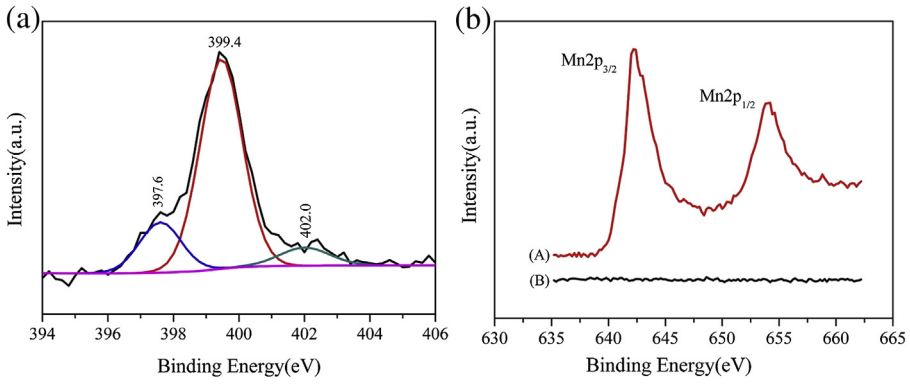

Fig. 2. (a) N 1s XPS spectra of MnO_2@PPy, (b) Mn 2p XPS spectra of (A) MnO_2 and (B) MnO_2@PPy coaxial nanotubes.

(Fig. 3b), all diffraction peaks are similar to that of the pristine α-MnO_2 nanotubes, confirming the presence of α-MnO_2 nanotubes in the composites after in-situ polymerization.

The structural information and chemical component of MnO_2@PPy coaxial nanotubes are also identified by the FT-IR spectroscopy. For comparison, the spectra for both α-MnO_2 and MnO_2@PPy coaxial nanotubes are recorded and shown in Fig. 4. It can be seen that from Fig. 4a, the characteristic peaks of α-MnO_2 appear at about 721, 531 and 475 cm^{-1}, belonging to Mn–O vibrations of MnO_6 octahedra in α-MnO_2 nanotubes [21, 44], and at 1635 cm^{-1}, relating to O–H vibrational mode of absorbed water. By contrast, in the spectrum of MnO_2@PPy coaxial nanotubes (Fig. 4b), the aforesaid peaks at 531 and 475 cm^{-1} shift to 527 and 469 cm^{-1}, respectively, and all display attenuation in intensity, reflecting a mutual interaction between PPy and MnO_2 that, most likely, is a hydrogen bond formed between oxygen atom of Mn–O and hydrogen atom of N–H in PPy. Furthermore, the characteristic peaks of PPy also appear in Fig. 4b. For example, the peak at about 1587 cm^{-1} is assigned to the symmetric stretching vibration of C=C bond in the PPy rings [45], the peaks at 1042 and 931 cm^{-1} are attributed to C–H deformation vibrations and C–H out-of-plane vibrations, respectively [45,46]. Such spectral information suggests that the PPy shell has been coated closely on MnO_2 surface and in doping state. The conductivity of MnO_2@PPy coaxial nanotubes measured at room temperature is 5×10^{-2} S cm^{-1}, enhancing nearly 100 times compared with that of α-MnO_2 (5×10^{-4} S cm^{-1}) and thus being consistent with the verdict of forming MnO_2@PPy coaxial nanotubes.

To further confirm the component of MnO_2@PPy, the thermal stability of the composites has been also characterized by TG measurement, as shown in Fig. 5. The initial weight loss of MnO_2@PPy coaxial nanotubes below 200 °C is 5.5 wt.%, which is attributed to the removal of the physically adsorbed water on the surface of the sample [29,47]. A further weight loss (44.8 wt.%) observed from 200 to 540 °C corresponds to the removal of doping anions and decomposition of PPy chain [29], indicating the weight percent of PPy is about 44.8 wt.%. A small weight loss (2 wt.%) between 540 and 800 °C relates to the decomposition of bonded hydroxyl groups of the structural water and the reduction of manganese from tetravalent to trivalent form accompanied by the loss of oxygen [28,29].

As a possible electrode material for supercapacitor application, the MnO_2@PPy coaxial nanotubes should optimize their morphology and microstructure, which have major impact on the electrochemical properties. It is found that the morphologies of the MnO_2@PPy coaxial nanotubes are dependent on the reaction acid concentration and the additional oxidant, such as $FeCl_3$. To be specific, the thickness of PPy shell can be controlled by adjusting the pH value. To better understand the formation of MnO_2@PPy coaxial nanostructure, acidity-dependent experiments are carried out firstly. As shown in Fig. 1a and 1c, the pure α-MnO_2 nanotubes display average diameter about 75 nm and smooth surfaces at the initial stage. By simply altering the concentration of sulfuric acid, the surface morphology of the MnO_2@PPy coaxial nanotubes can be varied gradually, as shown in Fig. 6. As the polymerization reaction is conducted in 0.001 M H_2SO_4, the surface of some 1-D

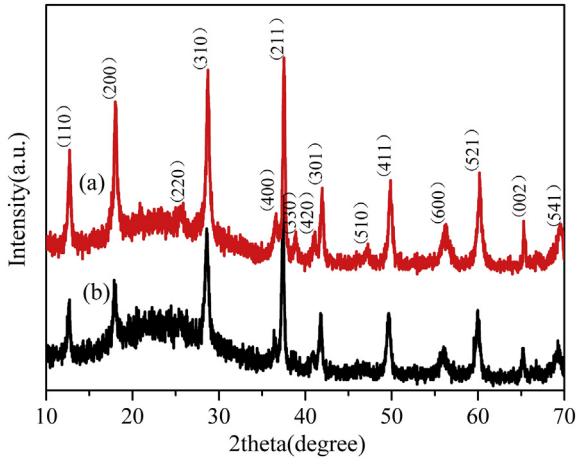

Fig. 3. X-ray diffraction patterns of (a) MnO_2, (b) MnO_2@PPy coaxial nanotubes.

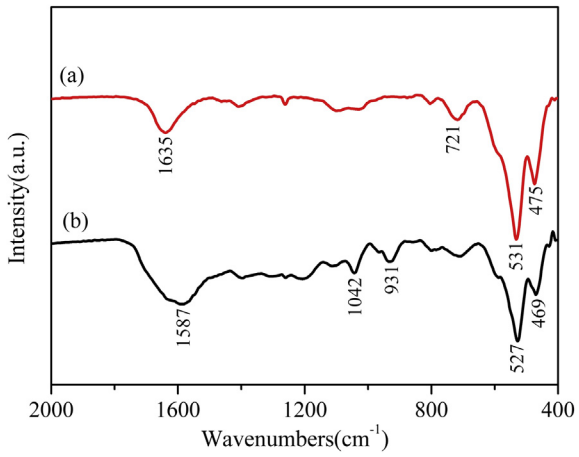

Fig. 4. FT-IR spectra of (a) MnO_2, (b) MnO_2@PPy nanotubes.

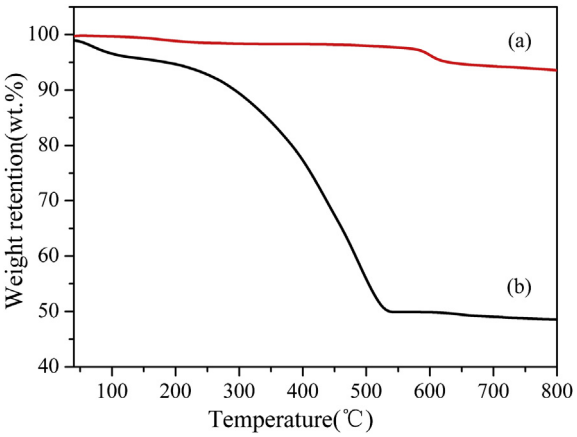

Fig. 5. TG curves of (a) MnO_2, (b) MnO_2@PPy coaxial nanotubes.

nanostructures becomes rough and some small particles appear (Fig. 6a), indicating that due to the fewer H^+, only a few of pyrrole monomers can be initiated by MnO_2 and H^+ to be polymerized. On the other hand, the amount of the H^+ also can increase the polymerization rate to influence the morphology of the product. Fig. 6b gives the FESEM image of MnO_2@PPy nanostructure, obtained in 0.1 M H_2SO_4. It can be noted that with increasing the amount of H^+, the surface of the product appears much rougher and the particles on surface become larger. When the concentration of H_2SO_4 increases to 1 M, owing to the rapid generation of PPy, the 1-D nanostructure of the product gets some damage as shown in Fig. 6c. Therefore, well-defined core/shell nanostructure, under the optimized H_2SO_4 concentration of 0.01 M, can be successfully prepared via in situ polymerization using α-MnO_2 nanotubes as template and oxidant.

The additional oxidant, such as $FeCl_3$, has a negative effect on the formation of MnO_2@PPy coaxial nanotubes. Fig. 6d shows the FESEM of MnO_2@PPy nanostructure synthesized by using $FeCl_3$ as an oxidant with the mole ratio of $FeCl_3$:pyrrole = 1:1. It can be seen that a large amount of separated PPy particles are obtained and deposited randomly on the surface of some α-MnO_2 nanotubes, showing that the products are mixture of α-MnO_2 and PPy. In such case, $FeCl_3$ oxidizes pyrrole monomers to be polymerized via homogeneous nucleation in bulky solution due to rapid polymerization rate. On the other hand, partial pyrrole monomers are also oxidized by α-MnO_2 and H^+, which comes from $FeCl_3$ hydrolysis, forming MnO_2@PPy coaxial nanostructure. It can be deduced that, in the absence of additional oxidant, appropriate amount of H^+ is critical for the formation of well-defined MnO_2@PPy coaxial nanotubes.

On the basis of above results, a possible formation mechanism of MnO_2@PPy coaxial nanotubes can be proposed, as illustrated in Fig. 7. It is understandable that the core of the coaxial nanotubes is α-MnO_2 and the shell is PPy. In our case, the α-MnO_2 nanotube surface exposed in acidic solution contacts with pyrrole monomers to proceed with a redox reaction. As the H^+ ions are added in the solution, some of them are adsorbed on the surface of α-MnO_2 nanotubes (the zeta potential is −20.8 mV) due to the electrostatic attraction. After adding pyrrole, the monomers transport to the surface of α-MnO_2 nanotubes because of their intrinsic hydrophilic characteristic in acid solution and polymerize over there, leading to the formation of PPy shell.

In order to study the electrochemical energy storage capacity of the as-synthesized MnO_2@PPy coaxial nanotubes, the samples made from α-MnO_2, pure PPy, and MnO_2@PPy nanotubes synthesized in 0.01 M H_2SO_4, are fabricated to supercapacitor electrodes and performed by cyclic voltammograms (CVs). As can be seen from Fig. 8a, MnO_2@PPy and pure PPy electrodes exhibit symmetric rectangular and enantiomorphous graphs, indicating the ideal capacitive behaviors. For the MnO_2 electrode, CV shape looks like slightly asymmetric rectangular graph between −0.2 and 0.8 V, manifesting the imperfect capacitive behavior, which may be attributed to the high oxidation potential of MnO_2 in neutral aqueous solution (pH = 7.8) [27]. Moreover, it is worth noting that the enclosed area of MnO_2@PPy electrode is larger than that of

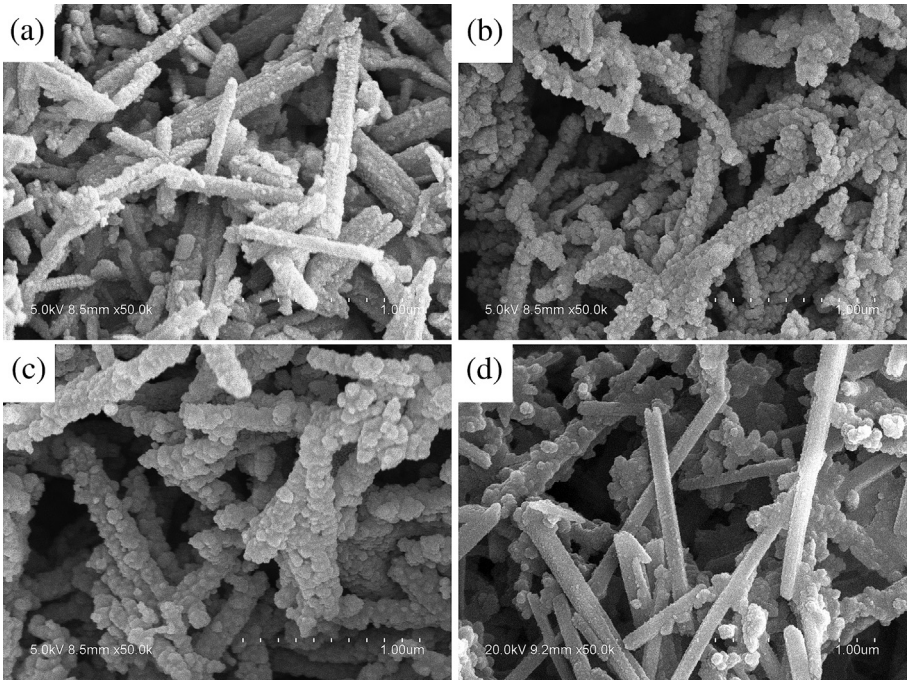

Fig. 6. FESEM images of MnO_2@PPy nanotubes synthesized under different conditions (a) 0.001 M H_2SO_4; (b) 0.1 M H_2SO_4; (c) 1 M H_2SO_4; (d) $FeCl_3$ as oxidant.

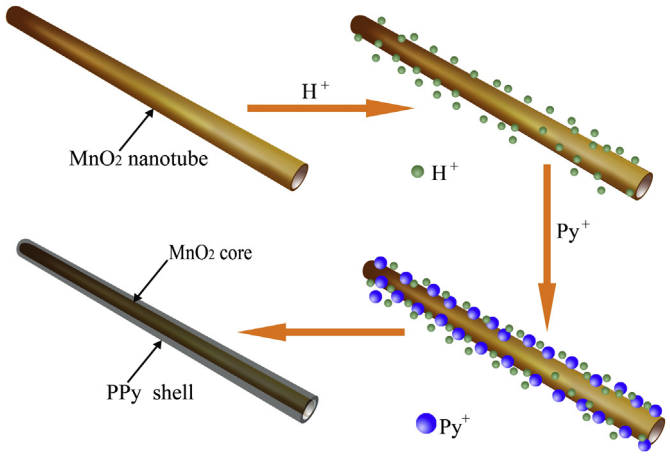

Fig. 7. Schematic illustration of the formation of MnO_2@PPy coaxial nanotubes in acid condition.

either pure α-MnO_2 or PPy electrode, indicating that MnO_2@PPy coaxial nanotubes have higher specific capacitance. Such excellent electrochemical properties of MnO_2@PPy coaxial nanotubes can be attributable to following reasons. First of all, the existence of highly electrical conductive PPy shell facilitates fast electron transport to MnO_2 core, overcoming the limitations of MnO_2 such as poor conductivity and low charge/discharge rates [6, 20]. Secondly, PPy has good electrochemical pseudocapacitive properties and specific capacitance is higher than MnO_2 [30]. Thirdly, PPy shell is coated on MnO_2 nanotubes to form one-dimensional ordered nanostructure, which can speed the ion diffusion in PPy phase and enhance utilization of electrode material [48]. Finally, chemical bonds between MnO_2 core and PPy shell, such as hydrogen bond interaction, decrease electron transfer barrier and increase the specific capacitance [28]. All the four aspects mentioned above lead to the high specific capacitance of the MnO_2@PPy electrode.

The cyclic voltammograms for α-MnO_2 and MnO_2@PPy coaxial nanotube electrodes at different scan rates are depicted in Fig. 8b and c, respectively. It can be found the CV curves are symmetric rectangular graphs, showing almost ideal capacitive behavior. The specific capacitances of MnO_2@PPy coaxial nanotubes calculated from Eq. (1) are 380, 346, 316, 287, 260, 233 F g^{-1} at the scan rates of 1, 2, 5, 10, 20 and 50 mV s^{-1} respectively, which double the specific capacitances of α-MnO_2 at each scan rate. With the increase of scan rate, specific capacitances of MnO_2@PPy coaxial nanotubes gradually decrease, as shown in Fig. 8d. In general, the redox reactions depend on the insertion/extraction rate of protons or alkali cations from the electrolyte. At lower scan rate, the working ions can reach almost all active areas, resulting in high-effective interaction between the ions and the electrode, and therefore, a good capacitive characteristic can be observed. As the scan rate is lower than 5 mV s^{-1}, a couple of redox peaks (P_c/P_a) can be observed on the CVs of MnO_2@PPy coaxial nanotubes (Fig. 8c), which stems from the redox transition of PPy, demonstrating that conducting PPy component makes more contribution to the capacitance, which lead to good capacitive characteristic [29]. On the contrary, higher scan rate decreases diffusion of ions into the interlayer of electrode, leading to a reduction in capacitance [15,35]. However, even at a scan rate as high as 50 mV s^{-1}, the specific capacitance still retains about 61.3%, indicating that MnO_2@PPy electrode possesses excellent rate capability.

The long-term cycle stability of electrode is of importance for practical applications. Fig. 9a demonstrates the specific capacitances as a function of cycle number at a scan rate of 50 mV s^{-1} in 1 M Na_2SO_4 for up to 1000 cycles. It is found that the specific

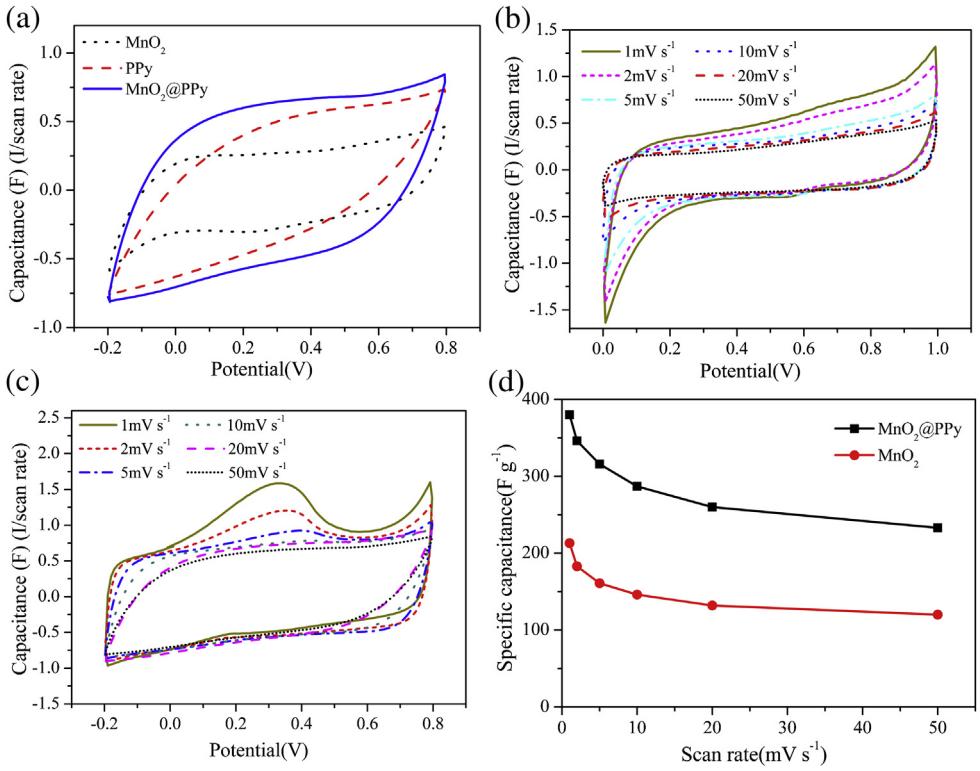

Fig. 8. CV curves of (a) MnO_2, pure PPy and MnO_2@PPy at 50 mV s^{-1}, CV curves of (b) MnO_2 and (c) MnO_2@PPy at different scan rates, (d) specific capacitances calculated from CV curves in (b) and (c).

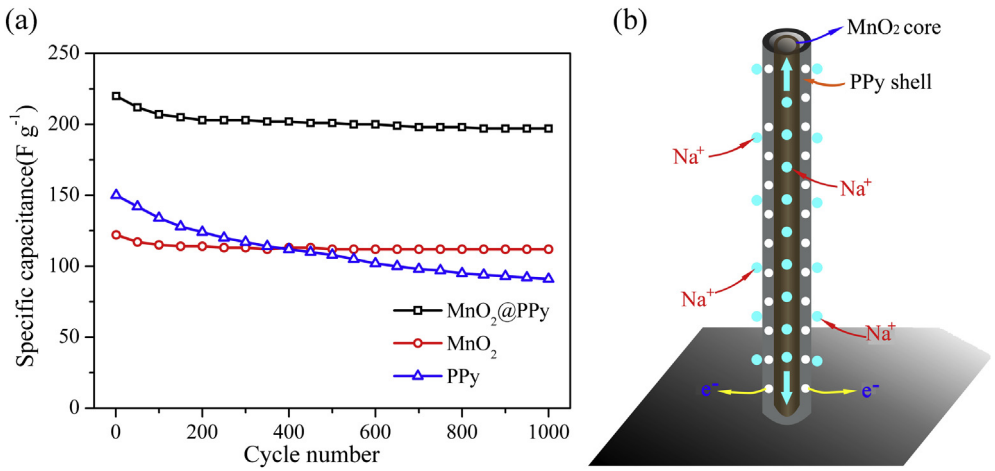

Fig. 9. (a) Specific capacitances as a function of cycle number at a scan rate of 50 mV s^{-1} in 1 M Na_2SO_4, (b) schematic of the charge storage advantage of the MnO_2@PPy coaxial nanotubes.

capacitances of pure PPy electrode decrease rapidly due to its structural change in cycle process, indicating its poor cyclability. It is gratifying that MnO_2@PPy coaxial nanotubes exhibit superior electrochemical stability with only 10% specific capacitances loss after 1000 cycles, which is similar to MnO_2. Such superior cyclic life is mainly attributed to the tube configuration of the MnO_2 core, which can not only serve as backbone for PPy, supplying the possible volume change during cycling, but also result in more contact area with the electrolyte. Furthermore, PPy shell, growing on MnO_2 nanotubes, can effectively enhance the conductivity of composites, speed electrons and ions diffusion. More significantly, the synergic effect between MnO_2 and PPy (Fig. 9b) mentioned above could inhibit the dissolution of MnO_2 and PPy, and consequently improve the electrochemical reversibility and stability of the composite electrode [6,8].

4. Conclusions

One-dimensional MnO_2@PPy composites with core/shell nanostructure are synthesized successfully via a simple and green approach without any surfactant and additional oxidant. MnO_2 nanotubes act as both template and oxidant under the acidic condition to prompt the polymerization of pyrrole on its fresh-activated surface. By changing the acid concentration, the thickness of PPy outer layer deposited on MnO_2 nanotubes can be adjusted. In the optimized experimental conditions, the as-prepared MnO_2@PPy coaxial nanotube electrode exhibits a high specific capacitance of 380 F g^{-1} (about two times of MnO_2) and a good cycling stability of 90% retention of the initial specific capacitance after 1000 cycles. The enhanced capacitive behaviors are attributed to the novel MnO_2@PPy coaxial nanostructure, confirming the feasibility of the rational design of electrode material for electrochemical capacitors.

Acknowledgments

This work was supported by the National Natural Science Foundation of China (No. 21174059), Open Project of State Key Laboratory of Superamolecular Structure and Materials (SKLSSM201308) and the Testing Foundation of Nanjing University.

References

[1] A.L.M. Reddy, M.M. Shaijumon, S.R. Gowda, P.M. Ajayan, Nano Lett. 9 (2009) 1002–1006.
[2] R. Liu, J. Duay, T. Lane, S.B. Lee, Phys. Chem. Chem. Phys. 12 (2010) 4309–4316.
[3] N.L. Kovtyukhova, T.E. Mallouk, Adv. Mater. 17 (2005) 187–192.
[4] Y.Y. Jiang, Y.Z. Lu, D.X. Han, Q.X. Zhang, L. Niu, Nanotechnology 23 (2012) 105609–105617.
[5] X.M. Wu, S.C. Zhang, L.L. Wang, Z.J. Du, H. Fang, Y.H. Ling, Z.H. Huang, J. Mater. Chem. 22 (2012) 11151–11158.
[6] R. Liu, S.B. Lee, J. Am. Chem. Soc. 130 (2008) 2942–2943.
[7] R. Liu, J. Duay, S.B. Lee, ACS Nano 4 (2010) 4299–4307.
[8] H. Jiang, C.Z. Li, T. Sun, J. Ma, Chem. Commun. 48 (2012) 2606–2608.
[9] M. Toupin, T. Brousse, D. Bélanger, Chem. Mater. 14 (2002) 3946–3952.
[10] X.C. Duan, J.Q. Yang, H.Y. Gao, J.M. Ma, L.F. Jiao, W.J. Zheng, CrystEngComm 14 (2012) 4196–4204.
[11] W. Xiao, H. Xia, J.Y.H. Fuh, L. Lu, J. Power Sources 193 (2009) 935–938.
[12] M.W. Xu, W. Jia, S.J. Bao, Z. Su, B. Dong, Electrochim. Acta 55 (2010) 5117–5122.
[13] O.A. Vargas, A. Caballero, L. Hernán, J. Morales, J. Power Sources 196 (2011) 3350–3354.
[14] H. Jiang, T. Zhao, J. Ma, C.Y. Yan, C.Z. Li, Chem. Commun. 47 (2011) 1264–1266.
[15] X.H. Tang, H.J. Li, Z.H. Liu, Z.P. Yang, Z.L. Wang, J. Power Sources 196 (2011) 855–859.
[16] S. Chen, J.W. Zhu, Q.F. Han, Z.J. Zheng, Y. Yang, X. Wang, Cryst. Growth Des. 9 (2009) 4356–4361.
[17] M. Toupin, T. Brousse, D. Bélanger, Chem. Mater. 16 (2004) 3184–3190.
[18] X.H. Tang, Z.H. Liu, C.X. Zhang, Z.P. Yang, Z.L. Wang, J. Power Sources 193 (2009) 939–943.
[19] J.F. Zang, X.D. Li, J. Mater. Chem. 21 (2011) 10965–10969.
[20] X.F. Yang, G.C. Wang, R.Y. Wang, X.W. Li, Electrochim. Acta 55 (2010) 5414–5419.
[21] J.R.I. Jafri, A.K. Mishra, S. Ramaprabhu, J. Mater. Chem. 21 (2011) 17601–17605.
[22] M.W. Xu, L.B. Kong, W. Zhou, H.L. Li, J. Phys. Chem. C 111 (2007) 19141–19147.
[23] W. Tang, Y.Y. Hou, X.J. Wang, Y. Bai, Y.S. Zhu, H. Sun, Y.B. Yue, Y.P. Wu, K. Zhu, R. Holze, J. Power Sources 197 (2012) 330–333.
[24] S.B. Ma, K.Y. Ahn, E.S. Lee, K.H. Oh, K.B. Kim, Carbon 45 (2007) 375–382.
[25] S.W. Lee, J. Kim, S. Chen, P.T. Hammond, S.H. Yang, ACS Nano 4 (2010) 3889–3896.
[26] H. Jiang, L.P. Yang, C.Z. Li, C.Y. Yan, P.S. Lee, J. Ma, Energy Environ. Sci. 4 (2011) 1813–1819.
[27] Z.H. Dong, Y.L. Wei, W. Shi, G.A. Zhang, Mater. Chem. Phys. 131 (2011) 529–534.
[28] W.B. Ni, D.C. Wang, Z.J. Huang, J.W. Zhao, G.E. Cui, Mater. Chem. Phys. 124 (2010) 1151–1154.
[29] J.G. Wang, Y. Yang, Z.H. Huang, F.Y. Kang, J. Power Sources 204 (2012) 236–243.
[30] R.K. Sharma, A.C. Rastogi, S.B. Desu, Electrochim. Acta 53 (2008) 7690–7695.
[31] J. Li, L. Cui, X.G. Zhang, Appl. Surf. Sci. 256 (2010) 4339–4343.
[32] H. Jiang, J. Ma, C.Z. Li, J. Mater, Chem. 22 (2012) 16939–16942.
[33] L. Chen, L.J. Sun, F. Luan, Y. Liang, Y. Li, X.X. Liu, J. Power Sources 195 (2010) 3742–3747.
[34] X. Zhang, L.Y. Ji, S.C. Zhang, W.S. Yang, J. Power Sources 173 (2007) 1017–1023.
[35] Q. Lu, Y.K. Zhou, J. Power Sources 196 (2011) 4088–4094.
[36] K. Wang, J.Y. Huang, Z.X. Wei, J. Phys. Chem. C 114 (2010) 8062–8067.
[37] J.L. Liu, M.Q. Zhou, L.Z. Fan, P. Li, X.H. Qu, Electrochim. Acta 55 (2010) 5819–5822.
[38] J. Zhang, X.H. Liu, L.X. Zhang, B.Q. Cao, S.H. Wu, Macromol. Rapid Commun. 34 (2013) 528–532.

[39] S.R. Sivakkumar, J.M. Ko, D.Y. Kim, B.C. Kim, G.G. Wallace, Electrochim. Acta 52 (2007) 7377–7385.
[40] R.K. Sharma, A. Karakoti, S. Seal, L. Zhai, J. Power Sources 195 (2010) 1256–1262.
[41] J.G. Wang, Y. Yang, Z.H. Huang, F.Y. Kang, J. Mater. Chem. 22 (2012) 16943–16949.
[42] J. Luo, H.T. Zhu, H.M. Fan, J.K. Liang, H.L. Shi, G.H. Rao, J.B. Li, Z.M. Du, Z.X. Shen, J. Phys. Chem. C 112 (2008) 12594–12598.
[43] K.L. Tan, T.G. Tan, E.T. Kang, K.G. Neoh, Y.K. Ong, Phys. Rev. B 42 (1990) 7563–7566.
[44] A.B. Yuan, Q.L. Zhang, Electrochem. Commun. 8 (2006) 1173–1178.
[45] T.Y. Dai, X.M. Yang, Y. Lu, Nanotechnology 17 (2006) 3028–3034.
[46] H.P.D. Oliveira, C.A.S. Andrade, C.P.D. Melo, J. Colloid Interface Sci. 319 (2008) 441–449.
[47] R.Z. Ma, Y.S. Bando, L.Q. Zhang, T. Sasaki, Adv. Mater. 16 (2004) 918–922.
[48] Y.G. Wang, H.Q. Li, Y.Y. Xia, Adv. Mater. 18 (2006) 2619–2623.